DOI 10.1007/s10946-020-09873-x
Journal of Russian Laser Research, Volume 41, Number 3, May, 2020

SIMULATION OF DISCHARGE CHARACTERISTICS FOR THE PLASMA ETCHING OF LARGE AREA SiO_2 SUBSTRATES

Jingwen Zhang,[1,2,3,4] Bin Fan,[1*] Zhiwei Li,[1] Guohan Gao,[1] Bincheng Li,[2] and Zhiwu Yan[1]

[1] *Institute of Optics and Electronics, Chinese Academy of Sciences Chengdu 610209, People's Republic of China*

[2] *School of Optoelectronic Science and Engineering University of Electronic Science and Technology of China Chengdu 610054, People's Republic of China*

[3] *University of Chinese Academy of Sciences Beijing 100049, People's Republic of China*

[4] *College of Energy and Power Engineering Lanzhou University of Technology Lanzhou 730050, People's Republic of China*

*Corresponding author e-mail: fanbin@ioe.ac.cn

Abstract

The electron density distribution and average electron temperature distribution in reactive ion etching (RIE) chamber are of great significance for the ionization and excitation reaction rate. The uniformity of radial distributions of the electron density and average electron temperature in the discharge chamber greatly affects the uniformity of the etching, especially the plasma etching of large area SiO_2 substrates. We study the effects of discharge conditions (including power and pressure) on the electron density and average electron temperature of plasma-etched 400 mm SiO_2 substrates in the reactive ion etching chamber; the simulation results show that the allowable major discharge conditions strongly affect the characteristics of plasma in the large area reactive ion etching chamber. Specifically, with increase in the power both the electron density and average electron temperature increase, being accompanied by deteriorating uniformity of their radial distributions. As the pressure increases, the electron density increases but average electron temperature decreases, being accompanied by deteriorating uniformity of their radial distributions. These methods and conclusions can provide reference for the improvement of cavity structure and large area RIE equipment designing and selection of the process parameters.

Keywords: reactive ion etching, capacitive coupled discharge, fluid simulation, discharge parameter, large area SiO_2 substrates, plasma radial uniformity.

1. Introduction

Traditional reflective space cameras (splicing, on-orbit assembly) have such technical bottlenecks as heavy weight, strict surface tolerance requirements, high manufacturing cost, and the difficulty of being folded and expanded, also their caliber is limited by launch [1, 2]. The diffractive imaging system with

Manuscript submitted by the authors in English first on February 5, 2020 and in final form on March 12, 2020.

the thin-film material as the objective lens has the characteristics of light weight, lower surface figure requirements, expandable space, etc., which provides a new idea for the development of super-aperture optical systems.

Micro–nano-structured thin-film optical technology is able to overcome the technical bottleneck of traditional optics and an effective way to achieve super-large caliber spaceborne imaging on the ground. Transmission of large-diameter micro–nano-structures is an important fabrication process in large-diameter thin-film optical systems [3–6]. Capacitively coupled plasma RF discharge is widely used in reactive ion etching process for the diffractive optical element fabricating [7, 8]. The high-energy electrons generated by RF discharge bombard the heavy particles and groups in the chamber to produce a large number of chemically active particles, which act as the main precursors for the gas phase and surface chemical reactions in the thin-film etching process [9, 10].

The reaction rate and uniformity are the key indices of the substrate manufacturing process, while the electron density and average electron temperature in the plasma directly affect the ionization and excitation reaction rate, and the uniformity of their radial distributions in the discharge chamber has a significant impact on the uniformity of thin-film etching [11]. Therefore, studying the influence of chamber structure and process parameters on the distribution of plasma characteristics in the reaction chamber is crucial for guiding the equipment design and process control [12, 13].

Reactive ion etching (RIE) is a typical etching technique for fabricating diffractive optical elements, and improving the uniformity of etching has always been a goal of optical fabricating [14]. The uniformity of radial distributions of the electron density and average electron temperature in the discharge chamber exerts a tremendous effect on the uniformity of the etching, especially the plasma etching of large area SiO_2 substrates. The discharge conditions and structure of the plasma process chamber determine the plasma distribution characteristics. Related research shows that the main factors affecting plasma discharge are RF power, RF frequency, gas pressure, electrode structure, electrode spacing, dielectric layer structure, material properties, etc. [15–18].

Most commercial RIE equipment is designed for substrates with a diameter of 300 mm or less. It is necessary to evaluate the influence of diameter increase and sample shape change of the equipment and technology when transferring the pattern of diffraction film optical elements in capacitively coupled plasma (CCP) equipment. The surge will affect the processing uniformity of the equipment for 300 mm substrates, and this effect will be more prominent if increasing the diameter to 400 mm and above [19]. Therefore, plasma distribution characteristics can be adjusted by changing related parameters and structures. In this paper, we study the influence of electrode power and pressure of a 400 mm substrate CCP discharge chamber on its electron density and average electron temperature based on COMSOL Multiphysics® program to guide subsequent substrate equipment design and process control.

2. Geometry Model

The plasma discharge room of the large area reactive ion etching chamber is a 2D axisymmetric structure model (as shown in Fig. 1), which is mainly composed of a power electrode, a substrate, a base, and a cavity. The substrate is made of SiO_2, which is an important optical material with a relative dielectric constant of 4. The substrate is 0.5 mm thick and placed above the power electrode. The cavity and the side are grounded. A power source is applied below the electrode, $V = V_0 \sin(2\pi f t)$, where RF frequency is $f = 13.56$ MHz. The pressure in the chamber p can be changed, the distance between the plates $d = 5.5$ cm, the radial monitoring line $z = 0.5\,d$, the radius of the chamber $r_1 = 45$ cm, the radius

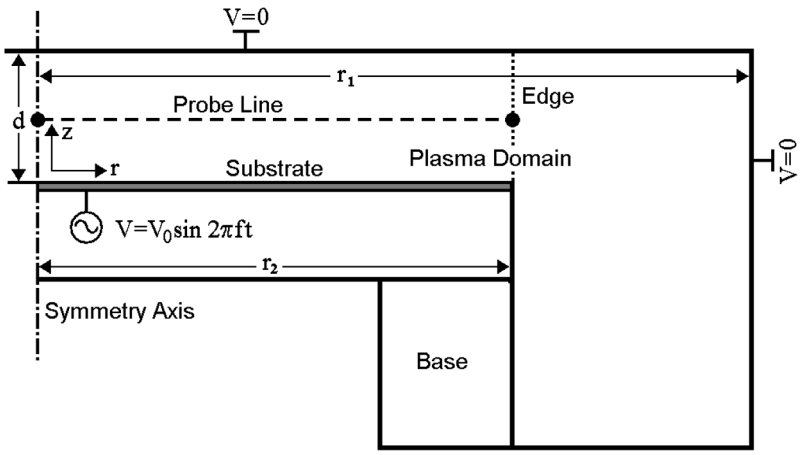

Fig. 1. Sketch of the chamber structure.

of the lower plate $r_2 = 32.5$ cm, the axial monitoring line $r = 0$, and the temperature $T = 300$K.

3. Governing Equations and Reactions

The traditional fluid model has been employed here in plasma simulations. The density and temperature of electrons are computed by solving electron drift-diffusion and electron energy equations.

Electron drift-diffusion equation reads [11, 20]

$$\frac{\partial n_e}{\partial t} + \nabla(-n_e\mu_e\mathbf{E} - D_e\nabla n_e) = \sum_{j=1}^{p_e} x_j k_j N_n n_e. \tag{1}$$

Electron energy equation is [11, 20]

$$\frac{\partial(3\,n_e kT_e/2)}{\partial t} + \frac{3\nabla\left[-n_e kT_e\mu_\varepsilon\mathbf{E} - kD_\varepsilon\nabla(n_eT_e)\right]}{2} + e\mathbf{E}\left(-n_e\mu_e\mathbf{E} - D_e\nabla n_e\right) + e\sum_{j=1}^{P_\varepsilon} x_j k_j N_n n_e \Delta\varepsilon_j = 0. \tag{2}$$

The Poisson equation describing electrostatic fields is as follows [11, 20]:

$$-\nabla\varepsilon_0\varepsilon_r\nabla V = q\left[\left(\sum_{k=1}^{P_i} Z_k n_k\right) - n_e\right], \tag{3}$$

where n_e is the electron density, μ_e is the electron mobility, D_e is the electron diffusion coefficient, $\mathbf{E}$ is the electric field vector, T_e is the electron temperature, μ_ε is the electron energy mobility, and D_ε is the electron energy diffusion coefficient. Based on the Einstein relation, the above correlation coefficients meet $D_e = \mu_e T_e$, $\mu_\varepsilon = (5/3)\,\mu_e$, and $D_\varepsilon = \mu_\varepsilon T_e$. Besides in the above equations, q is the unit charge amount, Z_k is the k^{th} heavy particle charge amount, n_k is its number density, x_j is mole fraction, N_n is the total neutral particle number density, and $\Delta\varepsilon_j$ is the energy loss of the electronic surface reaction. In addition, we calculated the rate coefficient of the reaction k_j, using the collision cross section

$$k_j = \sqrt{\frac{2q}{m_e}}\int_0^\infty \varepsilon\sigma_j(\varepsilon)f(\varepsilon)\,d\varepsilon, \tag{4}$$

where ε is the electron energy, m_e is the electron mass, $\sigma_j(\varepsilon)$ is the collision cross section, $f(\varepsilon)$ is the electron energy density function EEDF, and the Druyvesteyn distribution is used at low pressure [21,22].

Argon is an inert gas often used to analyze various characteristics of plasma due to its advantages of relatively simple plasma chemical composition and chemical reactions, no corrosion to the experimental system, and no pollution to the environment. In Table 1, we show seven gas reactions occurring in the chamber [10]; in addition, the surface reactions are shown in Table 2 [10], and the wall boundary conditions are shown in Table 3 [10].

Table 1. Plasma Reactions Involved.

Reaction	Formula	Type	$\Delta\varepsilon/V$
1	$e + Ar \rightarrow e + Ar$	Elastic	0
2	$e + Ar \rightarrow e + Ar^*$	Excitation	11.5
3	$e + Ar^* \rightarrow e + Ar$	Superelastic	–11.5
4	$e + Ar \rightarrow 2e + Ar^+$	Ionization	15.8
5	$e + Ar^* \rightarrow 2e + Ar^+$	Ionization	4.24
6	$Ar^* + Ar^* \rightarrow e + Ar + Ar^+$	Penning ionization	–
7	$Ar^* + Ar \rightarrow Ar + Ar$	Metastable quenching	–

Table 2. Reactions on the Plasma Surface.

Reaction	Formula	Sticking coefficient
1	$Ar^* \rightarrow Ar$	1
2	$Ar^+ \rightarrow Ar$	1

Table 3. Wall Boundary Conditions of the Plasma Surface Reactions.

Reflection coefficient	Forward sticking coefficient
0.05	1

4. Results and Discussion

4.1. Distributions of Electron Density and Average Electron Temperature

In this study, taking argon as the working gas, we used COMSOL Multiphysics® program to study the influence of discharge power and chamber pressure between two plates on electron density and electron temperature distributions of a large area reactive ion etching chamber model based on the average period algorithm. Figure 2 shows the contours of the electron density and average electron temperature distributions when the pressure of the chamber is 0.665 Pa, the radio frequency is 13.56 MHz, the distance between the plates is 0.055 m, and the electrode power P is 200 W. In Fig. 2 a, one can observe that the maximum of the electron density appears at the chamber center, and one can see clearly in Fig. 2 b that the electron temperature is distributed almost uniformly in the whole chamber, except for a maximum near the lower plate.

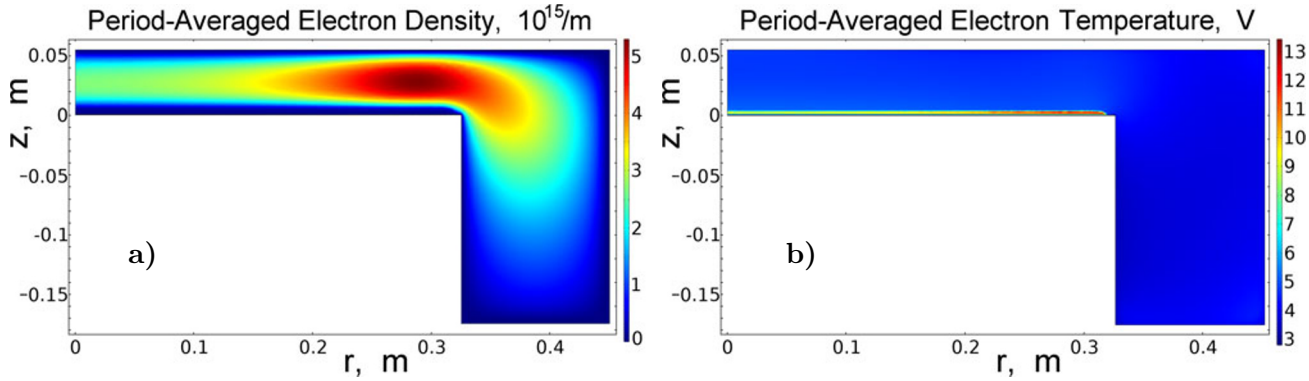

Fig. 2. Contours of the electron density and average electron temperature in a large-area reactive ion etching chamber.

4.2. Influence of Parameters

4.2.1. Power Effect

We studied the influence of different electrode powers (140, 160, 180, and 200 W) on the distribution of plasma characteristics under the following conditions: the pressure of the chamber is 0.665 Pa, the radio frequency is 13.56 MHz, and the distance between the plates is 0.055 m. The radial and axial distributions of the electron density between the two plates at different powers are shown in Fig. 3 a and b, respectively, and the radial and axial distributions of the average electron temperature between the two plates at different powers are shown in Fig. 3 c and d, respectively.

Under these conditions, one can see in Fig. 3 a that the radial electron density increases first and then decreases from the center to the edge of the chamber, and reaches the maximum value near the edge. Figure 3 b indicates that the electron density increases first and then decreases in the axial direction, and achieves the maximum in the middle of the plates. Figure 3 c shows that the radial average electron temperature decreases first and then increases from the center of the chamber to the edge, and a peak is observed near the edge before it drops sharply. It is shown in Fig. 3 d that the axial average electron temperature first increases sharply, then drops rapidly, and finally decreases slowly, reaching a minimum value at the polar plate and a higher peak value near the lower polar plate. The radial variation of the electron density is relatively remarkable. Both the electron density and the average electron temperature increase with increase in the power, but a change in the electron density is relatively more obvious.

4.2.2. Pressure Effect

We study the influence of different chamber pressure p (0.665, 1.33, 1.995, and 2.66 Pa) on the distribution of plasma characteristics under the following conditions: the RF power is 80 W, the frequency is 13.56 MHz, and the distance between the plates is 0.055 m. The radial and axial distributions of the electron density between the two plates at different pressures are shown in Fig. 4 a and b, respectively, and the radial and axial distributions of the average electron temperature between the two plates at different pressures are shown in Fig. 4 c and d, respectively.

Figure 4 a demonstrates that the radial electron density increases first and then decreases from the center of the chamber to the edge, and reaches a maximum near the edge of the lower electrode plate. In Fig. 4 b, one can see that the electron density increases first and then decreases in the axial direction, and

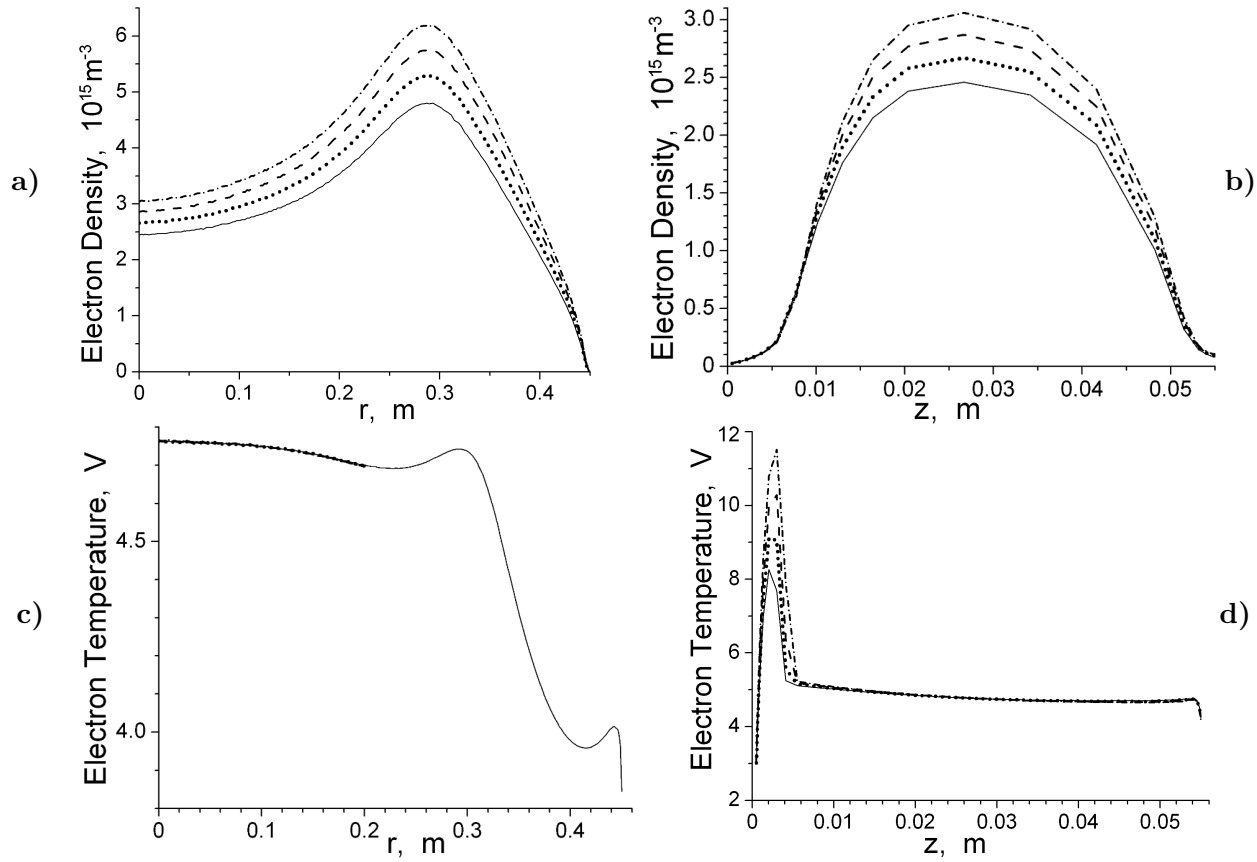

Fig. 3. The effect of the power on the electron density and average electron temperature. Here, solid curve stands for electrode power 140 W, 160 W (dotted curve), 180 W (dashed curve), and 200 W (dash-dotted curve).

achieves the maximum in the middle of the plates. Figure 4 c presents that the radial average electron temperature increases first and then decreases from the center of the chamber to the edge, and a peak occurs near the edge. Figure 4 d illustrates that the axial average electron temperature increases sharply, then drops substantially, and finally decreases slowly to the minimum at the lower plate, and a high peak exists near the lower plate. The change of radial electron density is relatively more significant. As the pressure increases, the electron density increases but the average electron temperature decreases.

4.3. Discussion of Simulation Results

In this paper, we studied separately the changes of electron density and average electron temperature with electrode power and gas pressure. Meanwhile, nonuniformity is defined, and the effects of electrode power and gas pressure on electron density and average electron temperature uniformity are analyzed [16, 23]. The nonuniformity definition for the curve in the two-dimensional axisymmetric model is shown in Eq. (5). In this paper, we focused on the uniformity of the 0 – 200 mm since the uniformity of the plasma is better in this range,

$$\mathrm{NU} = \frac{\int_{r_1}^{r_2}\int_{0}^{2\pi}\left|\dfrac{f-\bar{f}}{\bar{f}}\right| r\,dr\,d\theta}{\pi(r_2^2-r_1^2)}\,. \tag{5}$$

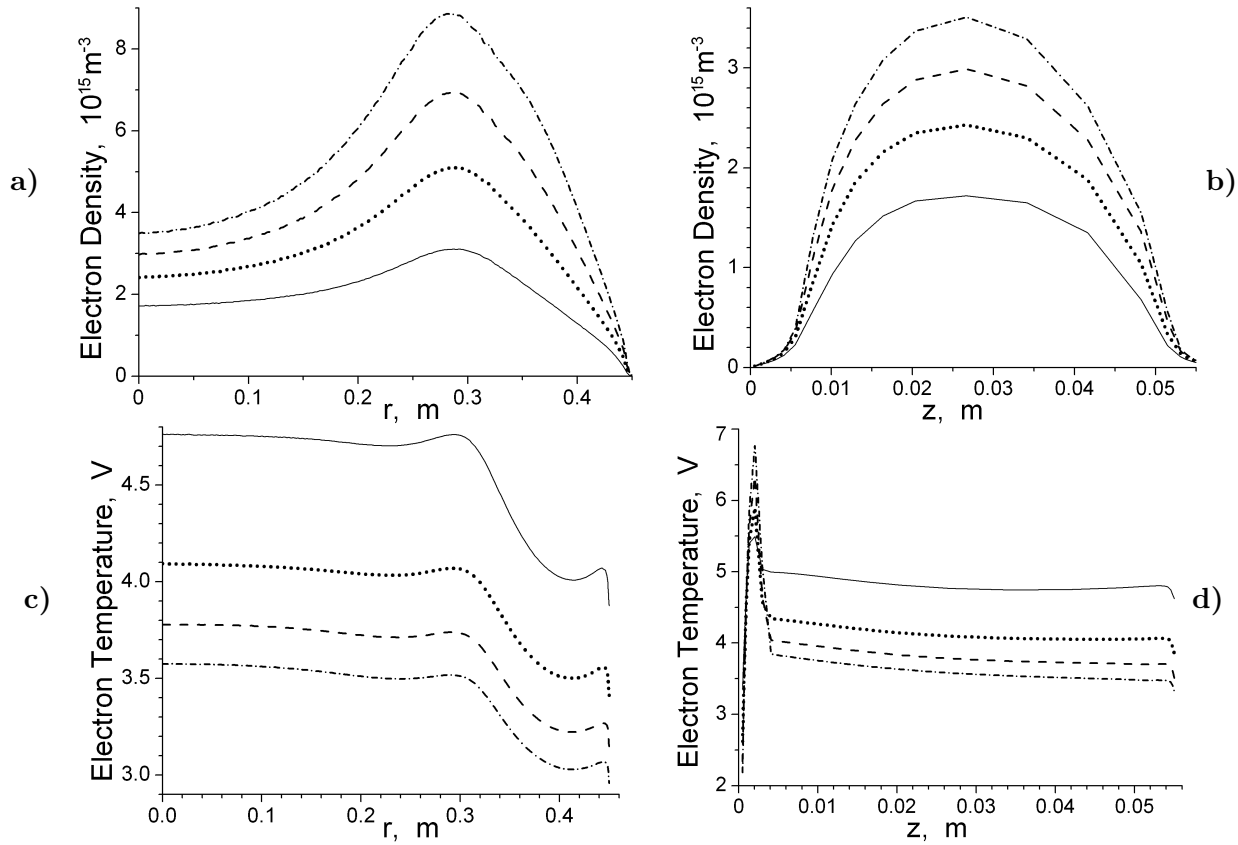

Fig. 4. The effect of the pressure on the electron density and average electron temperature. Here, $p = 0.665$ Pa (solid curve), $p = 1.33$ Pa (dotted curve), $p = 1.995$ Pa (dashed curve), and $p = 2.66$ Pa (dash-dotted curve).

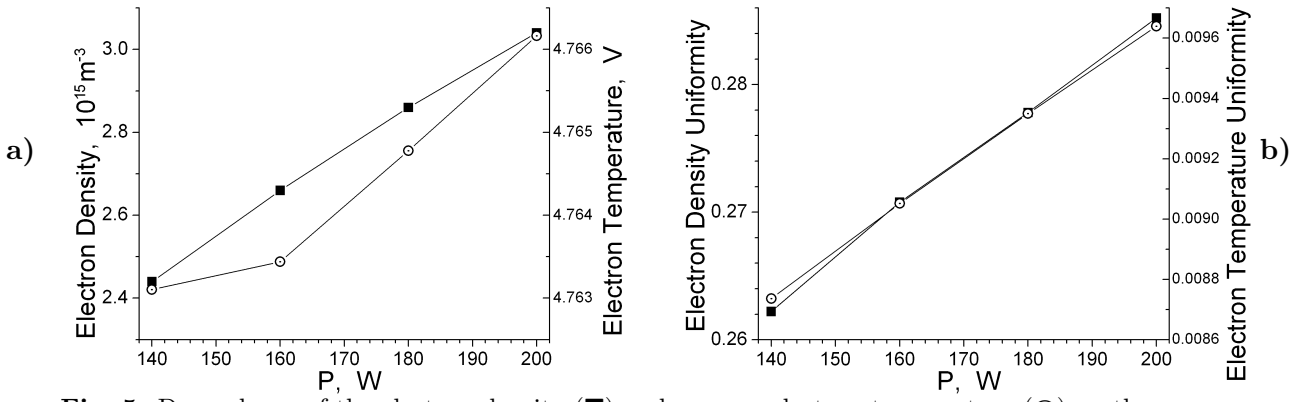

Fig. 5. Dependence of the electron density (■) and average electron temperature (⊙) on the power.

Figure 5 shows that with increase in the power, both the electron density and the average electron temperature increase, and both the uniformity of the electron density and the uniformity of the average electron temperature become worse.

From Fig. 6, one can obtain that with increase in the pressure, the electron density increases, the average electron temperature decreases, and both the uniformity of electron density and the uniformity of average electron temperature become worse.

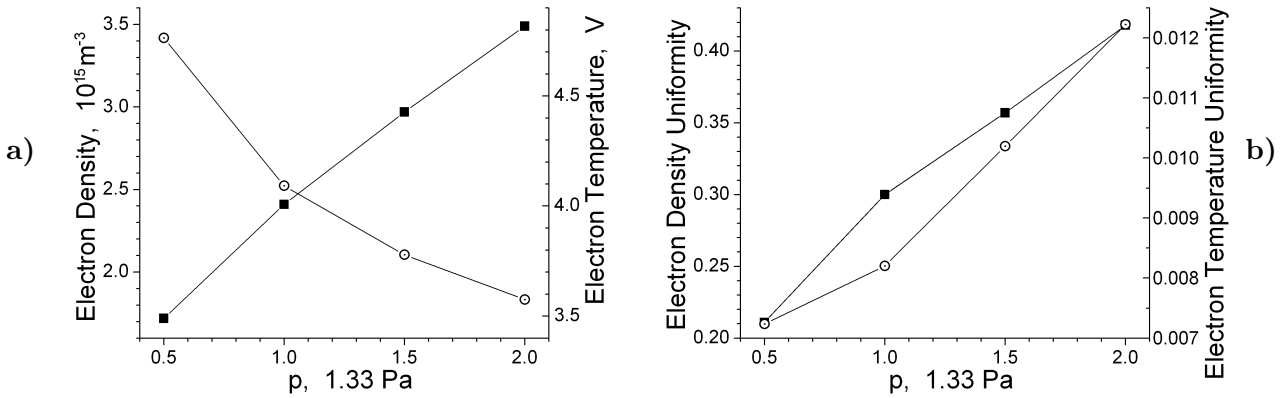

Fig. 6. Dependence of the electron density (■) and average electron temperature (⊙) distributions on the pressure.

4.4. Comparisons of Experiment Results

In order to verify the accuracy of the simulation algorithm, a silicon dioxide substrate was etched at a chamber with a RF power of 300 W and a gas pressure of 1.0 Pa; and the experimental data were measured. The radial distributions of the electron density and the average electron temperature are compared and analyzed. Figure 7 is an arrangement diagram of internal measuring points in the chamber, where the lower electrode plate in the chamber is above, and Fig. 8 discloses the experimental results.

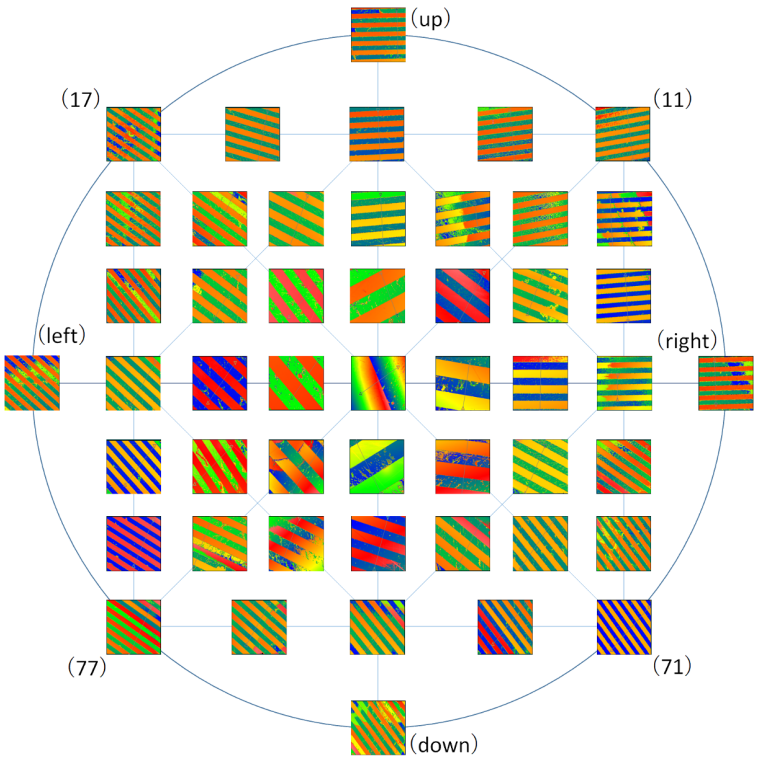

Fig. 7. Distribution of sampling points for measurement in the reactor chamber.

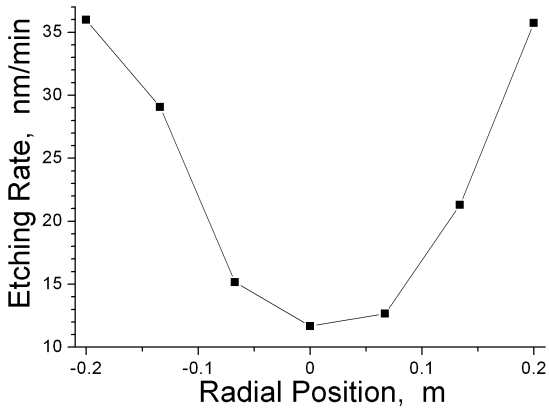

Fig. 8. Experimental results.

The electron density and average electron temperature distributions in the reactive ion etching (RIE) chamber are the direct causes of the ionization and excitation reaction rates. The uniformity of their radial distributions in discharge chamber significantly affects the uniformity of etching. The experimental results suggest that as the radius increases, both the etching rate and the electron density increase, but the average electron temperature decreases. It is worth noting that the electron density changes more significantly, and the changing trend of the etching rate in the radial direction is consistent with that of the electron number density distribution.

5. Conclusions

In this paper, we studied the axial and radial distributions of plasma electron density and average electron temperature in large area reactive ion etching chamber, as well as the influence of electrode power and chamber pressure on plasma discharge.

We found that under certain conditions, (1) the radial electron density increases first and then decreases from the center to the edge of the chamber, and reaches a maximum value near the edge; (2) the axial electron density decreases first and then increases, achieving a maximum in the middle of the plate; (3) the axial average electron temperature decreases from the center of the chamber to the edge first, then increases, and reaches a peak near the edge before it decreases sharply; (4) the axial average electron temperature increases sharply and then decreases rapidly, achieving a minimum value at the plate, and there is a higher peak near the lower plate; (5) the change of the radial electron density is relatively more significant.

Under different powers, both the electron density and the average electron temperature increase with the increasing power, but the change of the electron number density is more obvious; the uniformity of both the electron density and the average electron temperature becomes worse as the power increases.

Under different gas pressure, the electron density increases but the average electron temperature decreases with increase in pressure.

Experimental results show that both the etching rate and radial electron number density increase with the increasing radius.

Acknowledgments

This work was supported by the National Key R&D Program of China (2016YFB0500200).

References

1. J. M. Neauport, X. Ribeyre, J. M. Daurios, et al., *Appl. Opt.*, **42**, 2377 (2003).
2. Z. Zhao, H. Zhao, F. Gu, et al., *Opt. Express*, **22**, 5512 (2014).
3. P. D. Atcheson, J. Domber, K. Whiteaker, et al. "MOIRE: Initial demonstration of a transmissive diffractive membrane optic for large lightweight optical telescopes," Talk at the Space Telescopes and Instrumentation Conference (2012).
4. J. L. Domber, P. D. Atcheson, and J. Kommers, "MOIRE: Ground test bed results for a large membrane telescope," Talk at the Spacecraft Structures Conference (2014).
5. P. Atcheson, J. Domber, K. Whiteaker, et al., "MOIRE: Fround demonstration of a large aperture diffractive transmissive telescope," in: *Astronomical Telescopes Instrumentation*, *SPIE* (2014).

6. "Early J Solar Sail – Fresnel Zone Plate Lens for a Large Space Based Telescope" Talk at the 43rd AIAA/ASME/ASCE/AHS/ASC Structures, Structural Dynamics, and Materials Conference (2002).
7. S. Azimi, A. Sandoughsaz, and S. Mohajerzadeh, *J. Microelectr. Mech. Sys.*, **20**, 353 (2011).
8. J. Vukusic, J. Bengtsson, M. Ghisoni, et al., *Appl. Opt.*, **39**, 398 (2000).
9. G. E. Jie, L. Xuan, Y. I. Yang, et al., *Surface Rev. & Lett.*, **21**, 711 (2014).
10. M. A. Lieberman and A. J. Lichtenberg, *Principles of Plasma Discharges and Material Processing*, 2nd ed., Wiley, New York (2005).
11. W. Yang, X. P. Li, H. X. Xia, et al., *Chin. J. Vacuum Sci. Technol.*, **35**, 639 (2015) [in Chinese].
12. C. Jia, L. Ji, Z. Yu, et al., *J. Semiconductors*, **31**, 19 (2010).
13. K. Morikawa, K. Matsushita, and T. Tsukahara, *Analyt. Sci.*, **33**, 1453 (2017).
14. V. Georgieva and A. Bogaerts, *J. Appl. Phys.*, **98**, 3048 (2005).
15. Y. S. Liang, Y. R. Zhang, and Y. N. Wang, *Chin. Phys. B*, **25**, 244 (2016).
16. Y. S. Liang, Y. X. Liu, Y. R. Zhang, et al., *J. Appl. Phys.*, **117**, 043303 (2015).
17. X. Z. Jiang, Y. X. Liu, Z. H. Bi, et al., *Acta Phys. Sin.*, **61**, 15204 (2012).
18. Y. R. Zhang, X. Xu, A. Bogaerts, et al., *J. Phys. D: Appl. Phys.*, **45**, 218 (2011).
19. Y. Yang and M. J. Kushner, *J. Appl. Phys.*, **108**, 035003-2009 (2010).
20. Y. J. Hong, M. Yoon, F. Iza, et al., *J. Phys. D: Appl. Phys.*, **41**, 245208 (2008)
21. B. I. Jeon and H. Y. Chang, "EEDF measurements in dual frequency capacitively coupled plasma (CCP) and comparison with PIC simulation," Talk at the International Conference on Plasma Science (2003).
22. K. Sun, Y. Xin, X. J. Huang, et al., *Acta Phys. Sin.*, **57**, 6465 (2008) [in Chinese].
23. K. Zhao, Y. X. Liu, F. Gao, et al., *Phys. Plasmas*, **23**, 123512 (2016).